Journal of Materials Chemistry A

Accepted Manuscript

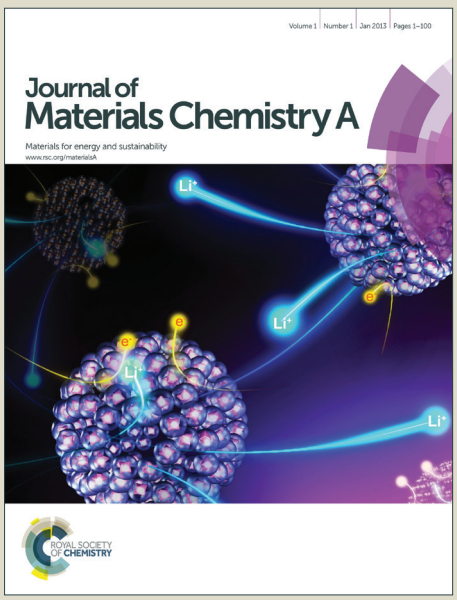

ROYAL SOCIETY OF CHEMISTRY

www.rsc.org/materialsA

Cite this: DOI: 10.1039/c0xx00000x

www.rsc.org/xxxxxx

ARTICLE TYPE

Enhanced capacitor effects in polyoxometalate/graphene nanohybrid materials; a synergetic approach to high performance energy storages

Keita Kume,[a] Naoya Kawasaki,[a] Heng Wang,[a] Tetsuya Yamada,[a, b] Hirofumi Yoshikawa*[a] and Kunio Awaga*[a, b]

Received (in XXX, XXX) Xth XXXXXXXXX 20XX, Accepted Xth XXXXXXXXX 20XX
DOI: 10.1039/b000000x

Synergic combination of a chemical redox reaction and a physical capacitor effect in one electrochemical cell is a promising route to realize both high-energy and high-power-density energy storage. In the present work, we studied the electrochemical properties of a nanohybrid system between polyoxometalate (POM) and graphene (RGO), in which individual POM molecules are adsorbed on the RGO surfaces. The molecular cluster battery (MCB) in which the POM/RGO hybrid was adopted as a cathode active material exhibited a higher battery capacity than the POM/SWNT (single-walled carbon nanotube)-MCB and the microcrystal POM-MCB. The observed capacity for the POM/RGO-MCB was found to be much larger than the theoretical one, as calculated from the redox change in POM, indicating a cooperative enhancement of the capacitor effects of RGO, induced by the POMs on the RGO surfaces.

Introduction

Electrochemical energy storage devices play an important role as a power source in portable electronic devices, electric vehicles, power grids, etc.[1] At present, the two major electrochemical energy devices are chemical batteries[2,3] and supercapacitors,[4,5] which work via different mechanisms. The charge/discharge processes of the chemical batteries are caused by the electrochemical redox reactions of electrode active-materials,[6] while the supercapacitors store electrostatic energy through the formation of electrical double layers (EDLs) at electrode interfaces.[7] Consequently, the batteries can possess much higher energy densities owing to the redox changes of battery active materials, while the power densities of the supercapacitors are higher, since the physical adsorption/desorption of ions at the electrode-electrolyte interfaces are much faster than the electrochemical reactions. Therefore, the synergic combination of a chemical redox reaction and a physical capacitor effect in one electrochemical cell would be a promising route to achieve both high energy and high power densities.[8]

Recently, we developed a new type of rechargeable battery, the molecular cluster battery (MCB),[9-14] which consists of a lithium metal as an anode and molecular clusters such as Mn12 clusters ($[Mn_{12}O_{12}(RCOO)_{16}(H_2O)_4]$, R = CH_3, C_6H_5, etc.) and polyoxometalates (POMs) as cathode active materials, in order to achieve both high capacity and rapid charge/discharge. Since the so-called Keggin-type POM, $TBA_3[PMo_{12}O_{40}]$ (TBA = tetrabutyl ammonium), possessed reversible, multi-electron redox properties, the MCBs of this compound exhibited a battery capacity of ca. 260 Ah per the unit weight (1 kg) of the cathode active material.[13, 15, 16] This capacity was higher than those of the usual lithium ion batteries (LIBs) (ca. 150 Ah/kg). Operando X-ray abso rption fine structure (XAFS) studies on the POM-MCBs demonstrated a twenty-four-electron reduction from $[PMo(VI)_{12}O_{40}]^{3-}$ to $[PMo(IV)_{12}O_{40}]^{27-}$during discharge,[13] which can explain the observed high battery capacity. Such electron sponge behavior indicates that the POMs are promising cathode active materials for high performance rechargeable batteries. However, since the cathode was a mixture of the microcrystals of

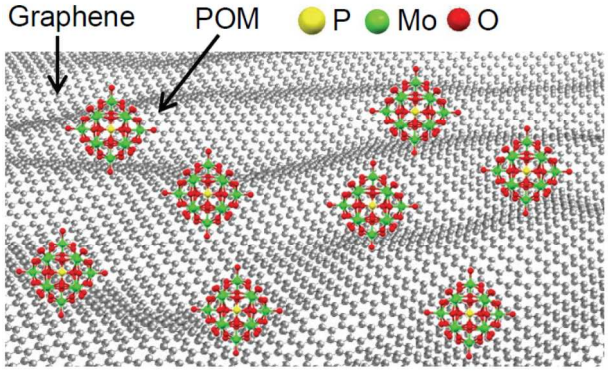

Fig. 1 Schematic view of the hybrid material between graphene and the Keggin-type polyoxometalate $[PMo_{12}O_{40}]^{3-}$ (POM). Although the IR spectra indicate the coexistence of the POM anions and the tetrabutyl ammonium (TBA) cations in the hybrid materials, the TBA cations are omitted for clarity.

[a]*Department of Chemistry & Research center for materials science, Nagoya University, Furo-cho, Chikusa-ku, Nagoya 464-8602, Japan E-mail: yoshikawah@mbox.chem.nagoya-u.ac.jp, awaga@mbox.chem.nagoya-u.ac.jp*
[b]*Core Research for Evolutional Science and Technology (CREST), Furocho, Chikusa-ku, Nagoya 464-8602, Japan*

† Electronic Supplementary Information (ESI) available: SEM and TEM images, Raman spectra, Charge/discharge curves, Operando Mo K-edge XANES spectra, First discharge curves and cycle performances, Power density plots. See DOI: 10.1039/b000000x/

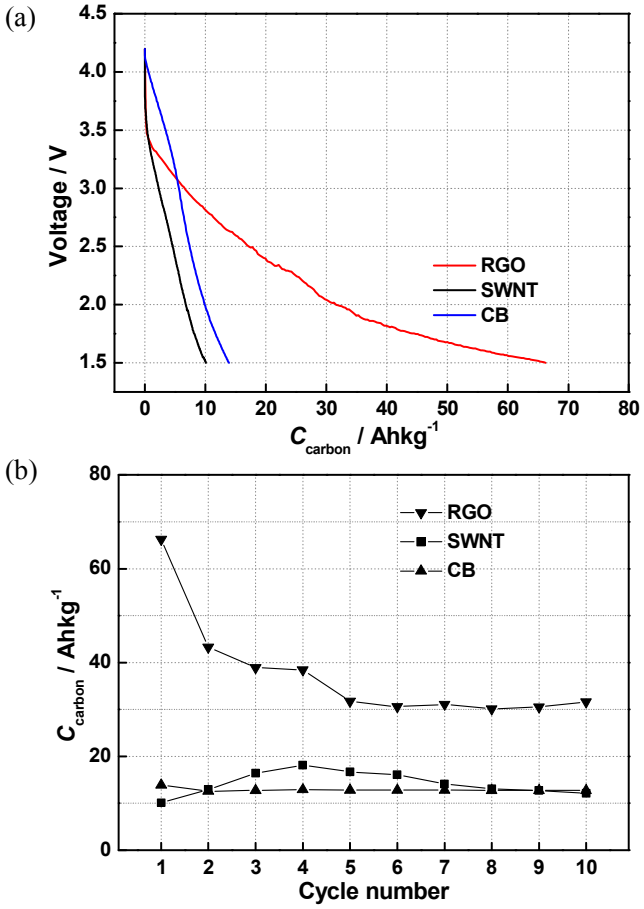

Fig. 2 First discharge curves (a) and the cycle dependence of the discharge capacities at 1.5 V (b) for RGO, SWNT and CB.

POMs and carbon black (CB) combined by a binder (see Fig. S1) in the initial experiments, the battery performance was considered to suffer from frictional penetration/removal of Li ions into/from the microcrystals and from non-smooth electron transfer between POMs and electrodes. To improve these drawbacks, we have developed nanohybrid materials consisting of the POMs and single-walled carbon nanotubes (SWNTs) in which the POM molecules were individually adsorbed on the SWNT surfaces.[12, 14] Actually, the performance of these POM/SWNT-nanohybrid MCBs was much improved in terms of both the capacity and charge/discharge rate, compared with those of the MCBs of the microcrystal POMs. It was strongly indicated that this improvement was caused by a capacitor effect due to the formation of EDLs at the interface of SWNTs.[12,14] Namely, the coexistence of a chemical redox reaction and physical capacitor effect was the most significant feature of the POM/SWNT-nanohybrid MCBs. It was expected that hybridization with the nanocarbon materials of larger interfaces would improve the energy storage capability, because, in general, an increase in the electrode surface area enhances the capacitoreffects.[17]

Graphene has attracted much interest due to its unique properties, including its chemical stability, high conductivity, and high mechanical strength.[18-21] It is theoretically considered that graphenes possess higher specific surface areas than SWNTs.[22-25] Among the various types of graphenes prepared by different

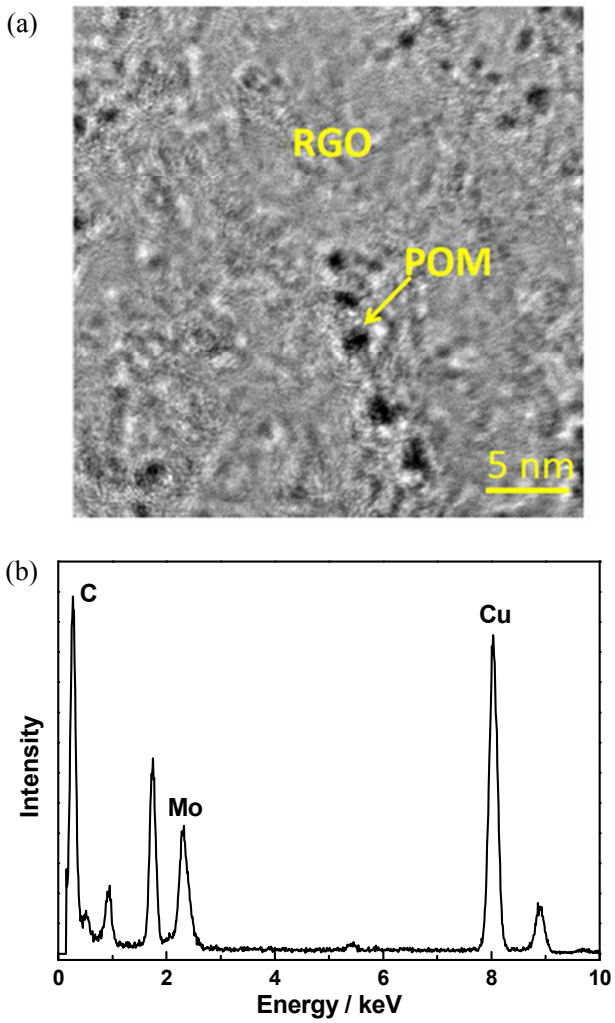

Fig. 3 TEM image (a) and EDX (b) for the POM/RGO hybrid materials.

methods,[26-28] the reduced graphene oxides (RGOs), which are obtained by liquid-phase reduction from graphene oxide, have promising advantages such as low cost and mass production.[29] In the present work, we prepared nanohybrid materials between POM and RGO (see Fig.1), and examined their performance as cathode active materials for MCBs. Although the electronic properties of the POM-integrated grapheme nanocomposites have been investigated in the context of their application to gas sensors and catalysis,[30-36] there has been no effort to develop rechargeable batteries with them. In this study, therefore, we will examine the cooperative energy-storage capability of these POM/RGO hybrid materials.

Experimental

Preparation method of POM and RGO.

Keggin-type POM, $TBA_3[PMo_{12}O_{40}]$ (TBA= $[N(CH_2CH_2CH_2CH_3)_4]^+$)(see Fig. 1), was prepared according to the method described in the literature.[37] RGO was also prepared using a previously reported procedure[29]: graphene oxide was prepared from graphite by a modified Hummers method,[38,39] and then it was reduced by hydrazine monohydrate to obtain RGO (see Fig. S2).

Preparation and characterization of the POM/RGO nanohybrid materials.

To graft the POM molecules onto the surfaces of RGO, an acetonitrile solution (5 ml) of $TBA_3[PMo_{12}O_{40}]$ (40 mg, 16 μmol) was added to a toluene suspension (100 ml) of the as-prepared RGO (80 mg) under vigorous stirring at room temperature. After stirring until the turbidity disappeared, the solution was filtrated using a membrane filter with a pore diameter of 0.1 μm. Finally, the precipitation was washed by toluene and dried in a vacuum. Since addition of the acetonitrile solution of TBA_3[POM] into the toluene suspension of RGO, resulted in a black precipitate with a colorless solution, all of the POMs were considered to be grafted onto the surfaces of RGO in this reaction to make the hybrid materials. This indicates that the weight ratio of TBA_3[POM] in them agrees with the preparation stoichiometry, namely 33 wt%.

Specific capacitance measurements of carbon materials.

Coin cells for each carbon material were fabricated in an inert atmosphere as follows. The cathode was made by mixing each carbon material and PVDF at a weight ratio of 80:20, where the weight ratio of PVDF was the same as that in the other batteries prepared in this work, while a lithium foil was used as the anode. The electrolyte was a solution of 1M $LiPF_6$ in ethylene carbonate (EC)/diethyl carbonate (DEC) (1:1, in weight).The charge/discharge measurements were carried out in the voltage range of 1.5 - 4.2 V on a Hokuto HJ1001-SM8A, with a constant current of I = 1.0 mA. The capacities are normalized by the weight of each carbon material.

Battery performance measurements of nanohybrid materials.

The 1:2 POM/RGO nanohybrid material was used as a cathode active material for MCBs to examine the battery performance. The cathode was made by mixing this hybrid material, CB, and polyvinylidenefluoride (PVDF) at a weight ratio of 30:50:20, as shown in Fig. 4(a). A lithium foil was used as the anode. The electrolyte was a solution of 1M $LiPF_6$ in ethylene carbonate (EC)/diethyl carbonate (DEC) (1:1, in weight). Battery coin-cells were fabricated in an inert atmosphere. For the control experiments, we also prepared the coin-cell MCBs of the 1:2 POM/SWNT nanohybrid material and of the POM microcrystals,[12, 13] though there was no nanohybridization in the latter. Note that, in these cathodes, the concentrations of the TBA_3[POM] were regulated so as to be the same (10 wt%, see Fig. 4(a)). The charge/discharge measurements were carried out in the voltage range of 1.5 - 4.2 V on a Hokuto HJ1001-SM8A, with a constant current of I = 1.0 mA.

Results and discussion

Before testing the performance of the POM/RGO materials as battery cathodes, we examined the specific capacitances—i.e., the electrostatic capacities—for CB, SWNT and RGO, which were the carbon materials used in the present work. The experimental details are given in the Supporting Information. Figure 2(a) shows their first discharge curves, in which the capacities, C_{carbon}, are normalized by the unit weight of each carbon material. The discharge voltages for CB and SWNT quickly decrease from 4.2 to 1.5 V, resulting in small capacities of less than 15 Ah/kg. Very small SWNT values of this sort are believed to be caused by a bundle structure.[37] In contrast, the voltage for RGO exhibits a slower decrease, and finally reaches 67 Ah/kg at 1.5 V. Figure 2(b) shows the cycle performance for the three carbon materials—namely, the discharge capacities in the first ten cycles. Although the values of C_{carbon} for CB and SWNT are constantly smaller than 20 Ah/kg, those for RGO remain over 30 Ah/kg after a quick decrease in the first five cycles. It is concluded that the

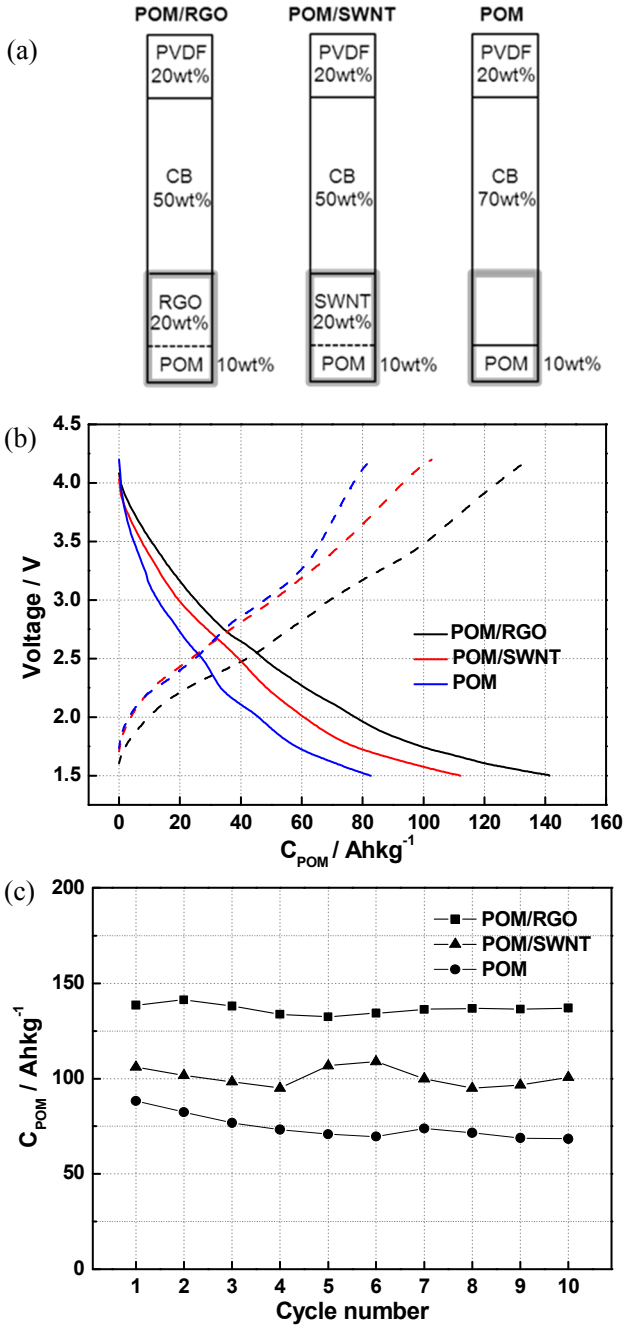

Fig. 4 (a) Cathode compositions for the POM/RGO-, the POM/SWNT, and the microcrystal POM-MCB. The broken lines in the POM/RGO-MCB and the POM/SWNT-MCB indicate nanohybridization between the two components. The 30 wt% of the cathode, indicated by the bold grey squares, is used for the normalization of the capacities. (b) Second charge/discharge curves for the POM/RGO-, the POM/SWNT, and the microcrystal POM-MCB. (c) Cycle performance for the POM/RGO-, the POM/SWNT, and the microcrystal POM-MCB.

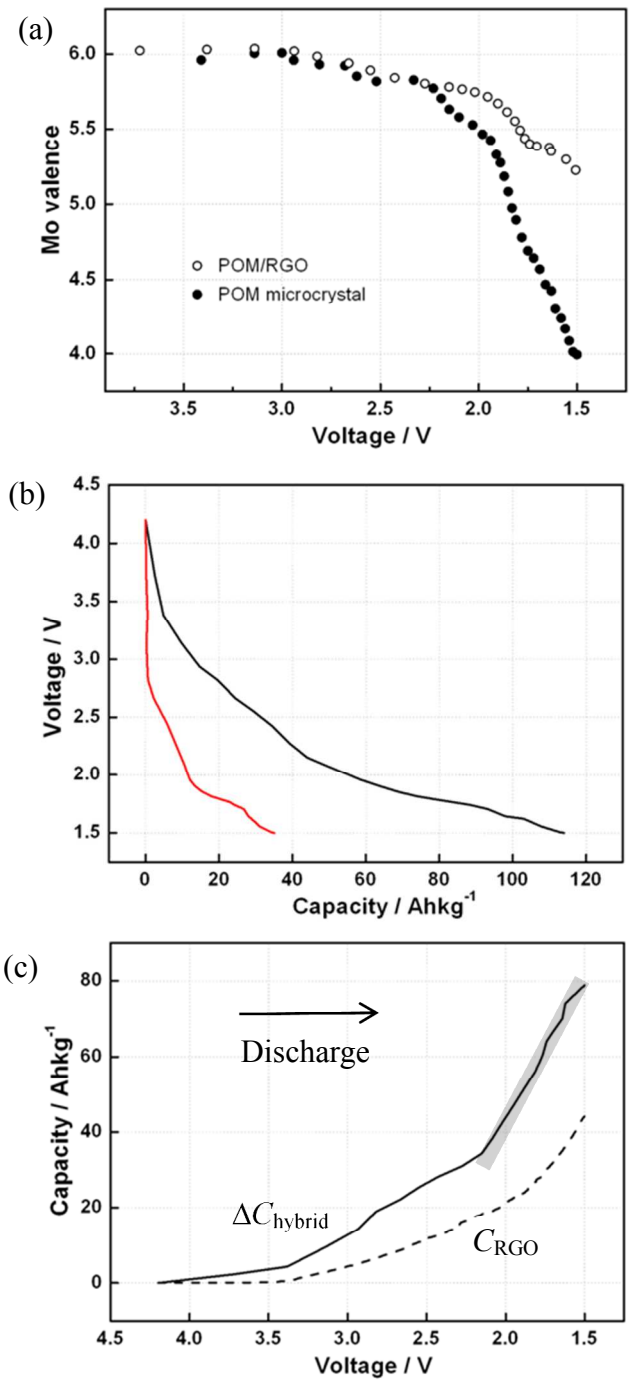

Fig. 5 (a) Averaged Mo valence of the POM molecule in the microcrystal POM-MCBs (closed circles) and in the POM/RGO-MCBs (open circles) as a function of the cell voltage. (b) Experimental discharge curve C_{hybrid}^{ex}(black) and calculated one C_{hybrid}^{red} (red) from the valence change in POM, for the POM/RGO-MCB. See the text. (c)Evolution of $\Delta C_{hybrid} = C_{hybrid}^{ex} - C_{hybrid}^{red}$ and C_{RGO} as a function of the battery voltage. The bold grey line is provided as a guide to highlight the significant increase in the gradient.

C_{carbon} value for RGO is much larger than those for CB and SWNT, as also reported previously.[24, 25, 40-42]

The POM/RGO nanohybrid materials, in which the weight ratio of $TBA_3[POM]$ was 33wt%, were prepared by using the same method as that previously reported for the POM/SWNT nanohybrid materials.[12,14] Figure 3(a) shows a transmission electron microscopy (TEM) image of the POM/RGO hybrid. Compared with the smooth surface of the as-prepared RGO (see Fig. S2), the surface of the POM/RGO hybrid looks rough, probably due to the presence of the TBA^+ cations, and is decorated by dark dots, whose diameters correspond to those of the individual and aggregated POM molecules. The individual POM molecules are separately grafted on the surface of the RGO sheet, although some POMs are aggregated on it. Figure 3(b) depicts the results of energy-dispersive X-ray (EDX) spectroscopy for the TEM image area shown in Fig. 3(a). This confirms the presence of molybdenum, as well as carbon, though the copper peaks are ascribed to the TEM grids. The IR and Raman spectra for the POM/RGO hybrid materials are shown in Figs. S3 and S4, respectively. They also indicate the presence of the $[PMo_{12}O_{40}]^{3-}$ anions with little structural change from that in $TBA_3[PMo_{12}O_{40}]$ and no significant change in the sp^2 domains of graphenes in the POM/RGO hybrid materials (see also Supporting Information). We roughly estimated the surface coverage of the POMs on the RGO surface as ca. 20 %, by calculating the surface area covered by the POMs in the TEM images.

Figure 4(b) shows the second charge/discharge curves for the MCBs of POM/RGO (black)and POM/SWNT(red), where the capacities C_{hybrid} are defined as those per the unit weight of the nanohybrid materials(namely, POM + nanocarbon), which occupy 30 wt% of the cathodes (see Fig. 4(a)). Since the first charge curve is very different from the others due to the fact that the as-prepared POM-MCBs are already in the charged state, we discuss the second charge/discharge curves as representative ones. The solid and broken curves in Fig. 4(b) indicate the discharge and charge processes, respectively. This figure also shows the data for the microcrystal POM-MCB (blue) for comparison, where the capacity is also defined per 30 wt% of the cathode (see Fig. 4(a)).Since there is no hybridization between POM and CB in this battery, and since the C_{carbon} of CB is small, the capacity of this MCB is considered to be mainly caused by the chemical redox of POM. All the charge/discharge curves in the initial 10 cycles for the three kinds of MCBs are shown in Fig. S5. As shown in Fig. 4(b), the discharge curves for the three batteries exhibit gradual voltage decreases from 4.0 V, but the values of C_{hybrid} at 1.5 V are significantly different: 140, 110 and 90 Ah/kg for the MCBs of the POM/RGO, POM/SWNT and POM microcrystals, respectively. Figure 4(c) shows the cycle dependence of the discharge capacities for the first ten cycles. It is concluded that the POM/RGO-MCB stably exhibits a larger capacity than the other two, even though the POM concentrations in them are the same (see Fig. 4(a)). This is probably caused by an enhanced capacitor effect in the POM/RGO-MCB.

To understand the enhanced capacity of the POM/RGO MCB, operando Mo *K*-edge XAFS measurements were carried out during the charge/discharge processes of the POM/RGO-MCB. The open circles in Fig. 5(a) show the averaged valence N_v of the Mo ions in this MCB during discharge, which were estimated from the edge energies of the Mo *K*-edge X-ray absorption near-edge structure (XANES) spectra (see Fig. S6). Figure 5(a) also shows the data for the microcrystal POM-MCB (closed circles), which were obtained previously.[13]The values of N_v for this MCB show a decrease from 6.0 to 4.0 in the voltage range of 3.5-1.5 V.

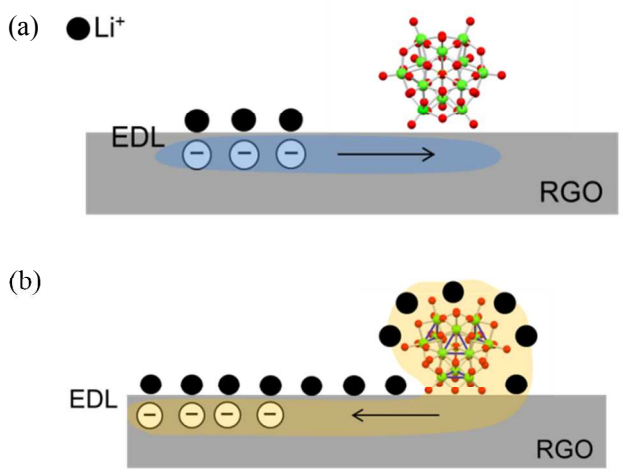

Fig. 6 Schematic view of the POM/RGO nanohybrid and Li^+ ions before (a) and after (b) the reduction of POM^{3-}. In (a), the negative charges on RGO in the EDLs interact with the POM^{3-}, and in (b), the negative charges of the super-reduced POMs (POM^{27-}) enhance the EDL formation.

This change in N_v by 2.0 means that all the $12Mo^{6+}$ ions in POM are reduced to Mo^{4+}; namely, one POM molecule can store 24 electrons. Actually, the battery capacity, calculated from this value for the 30 wt% fraction of the cathode, is ca.80 Ah/kg, which agrees with the observed battery capacity for the microcrystal POM-MCB (see Fig. 4(b)). In contrast, the POM/RGO-MCB exhibits a much smaller change in N_v; the initial value of 6.0decreasesto 5.2 at 1.5 V, indicating that the POM molecules are not fully reduced at this voltage. Although the battery capacity C_{hybrid} in the range of 4.0-1.5 V for the POM/RGO-MCB is much larger than that for the microcrystal POM-MCB, the contribution from the chemical redox change in POM is smaller in the former. This means that the enhanced capacity for the POM/RGO-MCB is caused by a significant increase in the capacitor effects, which overcomes the decrease in the redox capacity. In addition, the insufficient reduction in the POM/RGO-MCB suggests an interaction between POM and RGO in the nanohybrid, which increases the reduction potential of POM.

By using the values of N_v as a function of the battery voltage, as shown in Fig. 5(a), we calculated the theoretical discharge curve, C_{hybrid}^{red}, for the POM/RGO-MCB, which is solely caused by the redox reaction of POM. The results are shown as the red curve in Fig. 5(b), and are compared with the experimental results (C_{hybrid}^{ex}, black curve)—i.e., the second discharge curve for the POM/RGO-MCB, shown in Fig. 4(b). There is a significant difference between the two curves in the whole voltage range, 4.0-1.5 V. Figure 5(c) shows the battery-voltage dependence of the difference, namely $\Delta C_{hybrid} = C_{hybrid}^{ex} - C_{hybrid}^{red}$, which is considered to express the contribution from the capacitor effect due to the nanohybridization between TBA_3[POM] and RGO. The values of ΔC_{hybrid} gradually increase in the discharge process. As indicated by the bold grey line, there is a significant increase in the gradient below 2.2 V. This feature strongly suggests that the reduced species of POM would enhance the capacitor effect significantly. Figure 5(c) also shows the capacity of RGO (C_{RGO}, broken curve) for comparison, which was estimated from the values of C_{carbon} for RGO in Fig. 2(a). Since the weight of RGO is two-thirds of the weight of the hybrid, $C_{RGO} = (2/3)C_{carbon}$. The values of ΔC_{hybrid} are much larger than those of C_{RGO}, indicating that the presence of the POM molecules on the surfaces of RGO should greatly enhance the capacitor effect of RGO.

Next, we will discuss a possible mechanism for the cooperative capacity for the POM/RGO nanohybrid. The enhanced capacitor effects are associated with the electrochemical reaction between POM^{3-} (namely TBA_3[POM]) before discharge and POM^{27-} after it. Since the numbers of TBA^+ are much smaller than those of Li^+, the presence of the TBA^+ would not affect the interactions between POM and Li^+ significantly. Therefore, we ignore TBA^+ in the following discussion. Figure 6(a) shows the situation before the POM reduction, e.g., at 3.0 V, which consists of a POM^{3-} molecule and the EDLs between Li^+ ions and electrons on RGO. The increase in the reduction potential of POM is probably caused by the delocalized negative charges on RGO.[43] Figure 6(b) shows the situation after the reduction of POM^{3-}, which consists of a reduced POM and the EDLs. It is considered that the large negative charges on the POM would spread onto RGO and enhance the EDL capacitance significantly. This could explain the fact that ΔC_{hybrid} is significantly enhanced in the lower voltage range (see Fig. 5(c)). However, it is worth noting another possibility, i.e., that the adsorbed POM molecules might expand the spaces between the RGO sheets to accumulate more Li^+ ions.

Figures S7(a) and S7(b) show the load current-dependence of the first discharge curves and the cycle performances for the POM/RGO-MCB, respectively, at I = 1, 2, and 4 mA, in which the capacities are normalized by the unit-weight of the nanohybrid material(30 wt% of the cathode). With an increase in load current, the voltage drop during discharge occurs more quickly, but, even at I= 4mA, the discharge curve (solid, red) still indicates a capacity of 80 Ah/kg at 1.5 V, which is nearly the same as the capacity of the microcrystal POM- MCB at I = 1 mA (see Fig. 4(b)).This means that the nanohybridization with RGO can increase the charge/discharge rate of the POM MCB four-fold. The results for the POM/SWNT-MCB are shown in Fig. S8. The rate performance of this MCB is also improved, compared with the microcrystal MCB, but this improvement is much worse than that for the POM/RGO-MCB. Figure S9 shows the power densities for the POM/RGO-MCBs at I=1, 2 and 4 mA, which were estimated from Fig. S7(a) and the averaged discharge voltages. It is suggested that the power density monotonously increases with an increase in load current, finally reaching 700 W/kg at 4 mA, although this value is normalized by the nanohybrid weight (30wt% of the cathode). Since the capacity in the higher voltage range is not caused by the POM redox reaction but by the capacitor effects of RGO, larger power densities can be expected in the range of 3.0 - 4.0 V.[4,5]

Conclusions

In conclusion, we studied the electrochemical properties of the nanohybrid materials between POM and RGO, in which the individual POM molecules are adsorbed on the RGO surfaces. The charge/discharge measurements on the POM/RGO-MCB demonstrated a higher battery capacity and a faster charge/discharge rate than the corresponding ones for the microcrystal POM-MCB and the POM/SWNT-MCB. The fine analysis of the POM/RGO-MCB, based on the valence change in

POM and the capacitance of RGO, strongly indicated the cooperative enhancement of the capacitor effects in the POM/RGO hybrid materials. The present work suggests an excellent performance of POM as an additive for supercapacitors to enhance their capacity and a synergetic approach to combine a chemical battery and supercapacitor to realize high-energy and high-power density energy storages.

Acknowledgements

This work was performed with the approval of PF PAC (Proposal Nos. 2008G586, 2009G528, 2010G557, and 2012G027). The authors thank Prof. H. Shinohara, Dr. R. Kitaura, and Dr. R. Nakanishi of Nagoya University for their helpful assistance with the TEM measurements. This work was supported by a Grant-in-Aid for Scientific Research from the Ministry of Education, Culture, Sports, Science, and Technology (MEXT).

Notes and references

1 B. Dunn, H. Kamath and J-M. Tarascon, *Science*, 2011, **334**, 928-935.
2 M. Armand, and J-M. Tarascon, *Nature*, 2008, **451**, 652-657.
3 J-M. Tarascon and M. Armand, *Nature*, 2001, **414**, 359-367.
4 J. Zhang and X. S. Zhao, *ChemSusChem*, 2012, ***5***, 818-841.
5 G. Wang, L. Zhang and J. Zhang, *Chem. Soc. Rev.*, 2012, **41**, 797-828.
6 S. W. Lee, B. M. Gallant, H. R. Byon, P. T. Hammond and S. H. Yang, *Energy Environ. Sci.*, 2011, **4**, 1972-1985.
7 P. Bjoernbom, *Electrochem.Commun*., 2007, **9**, 211-215.
8 J. Kim and J. Cho, *Electrochem.Solid-State Lett*., 2007, **10**, A81-A84.
9 H. Yoshikawa, C. Kazama, K. Awaga, M. Satoh and J. Wada, *Chem. Commun*., 2007, **43**, 3169-3170.
10 H. Yoshikawa, S. Hamanaka, Y. Miyoshi, Y. Kondo, S. Shigematsu, N. Akutagawa, M. Sato, T. Yokoyama and K. Awaga, *Inorg.Chem*., 2009, **48**, 9057-9059.
11 H. Wang, S. Hamanaka, T. Yokoyama, H. Yoshikawa and K. Awaga, *Chem. Asian. J*., 2011, **6**, 1074-1079.
12 N. Kawasaki, H. Wang, R. Nakanishi, S. Hamanaka, R. Kitaura, H. Shinohara, T. Yokoyama, H. Yoshikawa and K. Awaga, *Angew. Chem. Int. Ed*., 2011, **50**, 3471-3474.
13 H. Wang, S. Hamanaka, Y. Nishimoto, S. Irle, T. Yokoyama, H. Yoshikawa, and K. Awaga, *J. Am. Chem. Soc.*, 2012, **134**, 4918-4924.
14 H. Wang, N. Kawasaki, T. Yokoyama, H. Yoshikawa and K. Awaga, *Dalton Trans.*, 2012, **41**, 9863-9866.
15 M. Lira-Canru and P. Gomez-Romero, *Chem. Mater.*, 1998, **10**, 698-704.
16 B. M. Azumi, T. Ishihara, H. Nishiguchi and Y. Takita, *Electrochemistry*, 2002, **70**, 869-874.
17 K. Fic, E. Frackowiak and F. Béguin, *J. Mater. Chem*., 2012, **22**, 24213-24223.
18 A. Abouimrane, O. C. Compton, K. Amine and S. Nguyen, *J. Phys. Chem. C*, 2010, **114**, 12800-12804.
19 C. Wang, D. Li, C. O. Too and G. Wallace, *Chem. Mater*., 2009, **21**, 2604-2606.
20 M. H. Liang and L. J. Zhi, *J. Mater. Chem*., 2009, **19**, 5871-5878.
21 S. J. Ding, D. Y. Luan, F. Y. C. Boey, J. S. Chen and X. W. Lou, *Chem. Commun.*, 2011, **47**, 7155-7157.
22 M. D. Stoller, S. Park, Y. Zhu, J. An and R. S. Ruoff, *Nano Lett*., 2008, **8**, 3498-3502.
23 K. H. Kim, Y. Oh, and M. F. Islam, *Adv. Funct. Mater*., 2013, **23**, 377-383.
24 D. Zhang, X. Zhang, Y. Chen, C. Wang and Y. Ma, *Electrochim. Acta*, 2012, **69**, 364-370.
25 J. Ye, H. Zhang, Y. Chen, Z. Cheng, L. Hu and Q. Ran, *J. Power Sources*, 2012, **212**, 105-110.
26 H. C. Schniepp, J. L. Li, M. J. McAllister, H. Sai, M. Herrera-Alonso, D. H. Adamson, R. K. Prud'homme, R. Car, D. A. Saville, I. A. Aksay, *J. Phys. Chem. B*, 2006, **110**, 8535-8539.
27 D. C. Wei, Y. Q. Liu, Y. Wang, H. L. Zhang, L. P. Huang and G. Yu, *Nano Lett*., 2009, **9**, 1752-1758.
28 Y.-F. Lee, K.-H. Chang, C.-C. Hu and Y.-H. Lee, *J. Mater. Chem.*, 2011, **21**, 14008-14012.
29 S. Park, J. An, J. R. Potts, A. Murali, S. Velamakanni and R. S. Ruoff, *Carbon*, 2011, **49**, 3019-3023.
30 S. Li, R. Liu, R. N. Biboum, B. Lepoittevin, G. Zhang, A. Dolbecq, P. Mialane and B. Keita, *Eur. J. Inorg. Chem*., 2013, 2013, 1882–1889.
31 J.-P. Tessonnier, S. Goubert-Renaudin, S. Alia, Y. Yan and M. A. Barteau, *Langmuir*, 2013, **29**, 393-402.
32 R. Liu, S. Li, X. Yu, G. Zhang, S. Zhang, J. Yao and L. Zhi, *J. Mater. Chem*., 2012, **22**, 3319-3322.
33 S. Wen, W. Guan, J. Wang, Z. Lang, L. Yan and Z. Su, *Dalton Trans*., 2012, **41**, 4602-4607.
34 J. Sloan, Z. Liu, K. Suenaga, N. R. Wilson, P. A. Pandey, L. M. Perkins, J. P. Rourke and I. J. Shannon, *Nano Lett.*, 2010, **10**, 4600-4606.
35 L. M. Rodriguez-Albelo, G. Rousseau, P. Mialane, J. Marrot, C. Mellot-Draznieks, A. R. Ruiz-Salvador, S. Li, R. Liu, G. Zhang, B. Keita and A. Dolbecq, *Daltom Trans*., 2012, **41**, 9989-9999.
36 C. Petit and T. J. Bandosz, *J. Phys. Chem. C*, 2009, **113**, 3800-3809.
37 C. Sanchez, J. Livage, J. P. Launay, M. Fournier and Y. Jeannin, *J. Am. Chem. Soc*., 1982, **104**, 3194-3202.
38 Q. Zeng, J. Cheng, L. Tang, X. Liu, Y. Liu, J. Li and J. Jiang, *Adv. Funct. Mater*., 2010, **20**, 3366-3372.
39 W. S. Hummers Jr. and R. E. Offeman, *J. Am. Chem. Soc*., 1958, **80**, 1339-1339.
40 F. Pico, J. M. Rojo, M. L. Sanjuan, A. Anson, A. M. Benito, M. A. Callejas, W. K. Maser and M. T. Martinez, *J. Electrochem. Soc*., 2004, **151**, A831-A837.
41 A. Lewandowski, P. Jakobczyk and M. Galinski, *Electrochim.Acta*, 2012, **86**, 225-231.
42 S. D. Cho, J. K. Im, H -K. Kim, H. S. Kim and H. S. Park, *Chem. Commun.*, 2012, **48**, 6381-6383.
43 C. Fleming. D.-L. Long, N. McMillan, J. Johnston, N. Bovet, V. Dhanak, N. Gadegaard, P. Kögerler, L. Cronin, N. Kadodwala, *Nature Nano*., 2008, **3**, 229-233.